Materials and Structures (2021)54:88
https://doi.org/10.1617/s11527-021-01670-5

ORIGINAL ARTICLE

Intra granular porosity of mineral powders: modeling and experimentation

Mohamed ElKarim Bouarroudj · Sébastien Rémond · Adèle Grellier · David Bulteel · Frederic Michel · Zengfeng Zhao · Luc Courard

Received: 24 May 2020 / Accepted: 24 February 2021

Abstract Recycled concrete aggregate (RCA) possess high water absorption, due to the porosity of the attached hardened cement paste they contain. Fine particles of RCA are composed of larger amounts of hardened cement paste, which makes their valorization even more difficult in concrete or mortar. One way to valorize these fine particles could be to use them as mineral addition, however their water absorption coefficient has to be determined, which is tricky for powders. The objective of this work is to estimate the remaining intra granular porosity of a ground powder using two different original approaches. The first modelling approach considers that the porous monolith material is composed of series of pores with characteristic volumes. A pore is considered opened due to grinding if it is cut by the surface of the particle and if its size is larger than the smallest inter granular pore. The remaining porosity after grinding is computed from the pore size distribution of the monolith material and the particle size distribution of the powder. The second experimental approach is based on mercury intrusion porosimetry tests performed on the powder. The separation between inter and intra granular porosity allows the estimation of the powder's remaining porosity. The obtained results show a good agreement between the two approaches in the case of disconnected pores. However, in the case of connected porosity, the experimental approach over estimates the amount of inter-granular porosity.

Keywords Modeling · Compaction · Bricks · Hardened cement paste · Grinding · Porosity

Abbreviations

RCA	Recycled concrete aggregate
MIP	Mercury intrusion porosimetry
WA	Water absorption
HCP	Hardened cement paste
GHCP	Ground hardened cement paste
LP	Limestone powder
GB	Ground brick
PSD	Particle size distribution
ρ_{abs}	Real density
γ_i	Volume fraction of grain size i
D_j	Diameter of grain i

M. E. Bouarroudj (✉) · A. Grellier · D. Bulteel
Centre for Materials and Processes, IMT Lille Douai, Institut Mines-Télécom, 59000 Lille, France
e-mail: bouarroudj.mohamedelkarim@gmail.com

M. E. Bouarroudj · A. Grellier · D. Bulteel · L. Courard
Junia, ULR 4515 - LGCgE – Laboratoire de Génie Civil et géoEnvironnement, Institut Mines-Télécom, Univ. Lille, Univ. Artois, 59000 Lille, France

M. E. Bouarroudj · A. Grellier · F. Michel · Z. Zhao
Urban and Environment Research Unit, ArGEnCo Department, GeMMe Building Materials, University of Liège, Liège, Belgium

S. Rémond
INSA CVL, LaMé, EA 7494, Univ Orléans, Univ Tours, Orléans, France

Published online: 31 March 2021

ρ_{app}	Apparent density
P	Bulk density
V_{cp}	Characteristic pore volume
R	Grain radius
ρ_c	Density of pore centers
P	Mercury pressure
ϕ	Initial porosity of the monolith material
dv	Elementary volume
dN_c	Number of pore centers
dV_p	Elementary volume of pore
ϕ_r	Remaining porosity
x_i	Volume fraction of each size of pores
$R_{5\%}$	Radius of 5% of the passing particle
γ_{total}	Packing density
V_s	Solid volume
V_{0-} V_{inject}	Total volume of the packing for a given pressure of mercury
γ_∞	Final packing density
$\Delta\gamma_\infty$	Variation of packing density
t	Number of taps
τ	Characteristic time
β	Fitting parameter
$V_{envelope}$	Envelope volume of grains
R^2	Correlation coefficient

1 Introduction

Sustainable development is becoming a strategic issue in the construction sector. This sector is responsible for 25% of the total CO_2 emissions, and uses 50% of the natural resources [1]. To reduce these emissions, replacing a part of the clinker in cement fabrication by mineral addition, such as limestone filler fly ash…, and replacing part of the cement by industrial by-product when manufacturing concrete is a good method [2, 3]. Reusing recycled concrete aggregates for the manufacture of new concrete can be an alternative to reduce both the consumption of natural resources and the amount of wastes that has to be disposed [1–4].

Recycled concrete aggregate (RCA) is composed of a mix between natural aggregate and attached old cement paste. RCA presents a high water absorption (4–12%) and low density (2.1 and 2.5 g/cm^3) due to the porosity present in the cement paste [5]. The fraction larger than 4 mm is easy to valorize in the construction sector. The literature review [6–13] shows that using particles lower than 4 mm in concrete presents difficulties on controlling the fresh and hardened behavior of concrete or mortar due to the high water absorption caused by a high presence of cement paste. Until now, research on RCA are focused more on using RCA as aggregate [6–8] than as a mineral addition in concrete [14, 15] or as a substitution of clinker in cement fabrication [16].

Incorporating fine particles (< 150 μm) of RCA in concrete presents a challenge to face. The cement paste is the most porous part of RCA and it is more abundant in fine particles than in coarser ones [17, 18]. Oksri-Nelfia et al. [14] and Bordy et al. [15] suggest to use that fraction as mineral addition in concrete. The authors studied the effect of replacing a part of cement by a model ground fine RCA composed of cement paste. The results show that using ground model RCA as mineral addition is possible up to 25% of cement volume replacement. In these research works the authors do not consider the porosity of the ground RCA, which is probably still present. This porosity, and the water absorption that goes with it, could influence significantly the fresh and hardened properties of concrete made with these powders. Indeed, the effective water in concrete is defined as the water that is present in the cement paste (the available water for cement hydration) [19, 20]. However, when a porous mineral addition is used, part of this water is absorbed which decreases the amount of water available for cement hydration and for the fluidification of the fresh mixture. In a similar research Bouarroudj et al. [21] take into consideration the intra granular porosity present in the ground model RCA (composed from hardened cement paste) to correct the amount of water introduced into the mix. They show that substituting the cement by ground RCA with taking into account the water absorption of the powder allows controlling the effective water and maintain the fluidity of the mix.

So, knowing the water absorption (or the water accessible porosity) of RCA is of a great importance to formulate concrete. Different methods exist to measure that porosity of coarse granular materials. For example, the mercury intrusion porosimetry (MIP) allows knowing the porosity and the size distribution of pores larger than 7 nm. Also, several experimental methods exist for the measurement of water accessible porosity of aggregates such as EN 1097-6 [22], ASTM C 128-04 [23], IFSTTAR N°78 [24]. However, these

experimental methods are not applicable to fine granular materials. Zhao et al. [25] and Le et al.[26] showed that using standard EN 1097-6 [22] or IFSTTAR [24] protocols to measure the porosity is not accurate for particles lower than 0.5 mm. The small size of grains prevents in that case from separating particles from one to another which does not allow distinguishing intra and inter granular porosities. Moreover, in the case of powders, the measurement is complicated due to the fast water absorption [27]. Strømme Mattsson et al. [28] developed a method based on ionic mobility in dielectric systems for the measurement of the porosity of glass beads and cellulose agglomerates powders. However, this method cannot be applied to mineral powders, because of ions that can be released by the material. To our knowledge, there is currently no method allowing the measurement of intra granular porosity of mineral powders.

The objective of this work is to propose alternative methods allowing the assessment of the intra granular porosity of mineral powders. To achieve this objective, three different types of mineral additions are used: limestone filler, ground hardened cement paste, and ground brick. The use of these materials allows to study mineral additions with different porosities, pore size distributions and connectivities of pores.

Two original approaches are proposed. The first one is based on a theoretical model that allows estimating the porosity of ground porous materials, from the pore size distribution of the monolith material (material before grinding) and the particle size distribution of the powder. For the second approach, the porosity of the porous powder is estimated by means of MIP test.

The paper is organized as follows. First the used materials and their characteristics are presented. Then, the theoretical model is described in Sect. 3 and applied to two porous ground materials. The experimental approach is presented in Sect. 4. Conclusions and perspectives are formulated in Sect. 5.

2 Materials preparation and characterization

2.1 Materials preparation

Three different powders have been used. The first one is a commercial Limestone Powder (LP) provided by Carmeuse, Belgium. According to the manufacturer, the porosity of the original limestone from which the LP is produced is less or equal to 1%. The second is a ground hardened cement paste (GHCP) and the third one is ground brick (GB). The GHCP and GB are mineral additions produced from HCP and brick, which can be considered as model materials for CDWs (as in [14–21]). The LP is used as a reference mineral addition and supposed non-porous. The used materials present clearly different pore size distributions, which will make possible to test the modeling and experimentation procedure.

The HCP is manufactured using cement CEM I 52.5 N from CBR Heidelberger cement (Belgium), complying with standard EN 197-1 [29]. The water to cement ratio is 0.5. To ensure a good homogenization during the manufacturing of the cement paste, half of the cement's quantity is first added to the water and mixed for 90 s, after that the other half is added and the mixing process continues for 90 more seconds. Thereafter, the fresh cement paste is poured in 1 L hermetic plastic bottles. The cement paste is gently vibrated to minimize the presence of air bubbles. In the end, the fresh cement paste is sealed and rotated continuously during 6 h (until setting) using a proper rotating machine in order to avoid segregation and bleeding. The hardened cement paste (HCP) is stored at 20 °C in the sealed bottles during 90 days to ensure a high hydration degree[30, 31].

Bricks are provided from the Barry division plant of Ploegsteert company in Belgium.

The grinding procedure of both the HCP and the brick is made of two steps. In the first step, the material is crushed using a jaw crusher with an opening size of 8 mm to have a particle size ranging between 4 and 20 mm. These coarse particles will be used for further characterization of the monolith HCP and brick. In the second step, the material is ground using a ball mill in order to get a fine powder (ground hardened cement paste: GHCP, ground brick: GB) of dimensions lower than 300 μm.

In order to have a close particle size distributions (PSD) between the LP and both GHCP and GB, the obtained powders are ground several times using a disc crusher, until PSDs are similar.

First MIP test is made on the monolith HCP and brick, on coarse particles produced from the first crushing operation. After that, characteristics of the 3 powders are measured (PSD, specific surface area by

BET and Blaine methods, helium density). Finally MIP is carried out on GHCP, GB and LP.

2.2 Characterization protocol

For determining the porosity and the pore size distribution of the monolithic HCP and brick, a Micrometritics autopore IV with a mercury pressure ranging between 0 and 200 MPa is used. Five tests are performed with samples of approximately $1 \times 1 \times 1$ cm^3.

For the ground powders, the PSD is determined with laser granulometer (Mastersizer 2000) using Fraunhofer model [32]. Because of the anhydrous particles eventually present in GHCP, the laser granulometer tests are performed in ethanol for all powders. The specific surface area (SSA) is determined with 3 different methods: according to standard EN 196-6 [33] (Blaine fineness), with BET method (micrometritics 3D FLEX surface characterization), and computed from the PSD considering spherical non-porous particles (Eq. 1), where γ_j is the volume fraction of grain size j, ρ_{abs} is the real density obtained with helium pycnometer, D_j is the diameter of the grain:

$$SSA_{computed} = \sum_{j=0}^{n} \left[\frac{\gamma_j \times 6}{\rho_{abs} \times D_j} \right] \quad (1)$$

2.3 Characterization results

Table 1 presents the porosity, apparent density (ρ_{app}), and bulk density (ρ) obtained with the MIP analyses performed on the monolith material. The porosity of the monolith limestone is much smaller than those of brick and HCP and can be neglected. The MIP tests on various samples of HCP and brick (monolith) showed that HCP and brick are homogeneous. Figure 1 presents the pore size distributions of HCP and brick. The diameter of the median pore of HCP is about 0.07 µm, and that of largest one is around 0.7 µm. The critical pore diameter where the mercury intrusion starts to increase sharply is about 0.18 µm. For the brick, the median pore is about 3 µm, and the largest one is around 4 µm. The critical pore diameter where the mercury intrusion starts to increase sharply is about 1 µm. An important difference in the pore sizes is observed between the brick and HCP.

The particle size distributions of the three powders are presented in Fig. 2. Given the grinding procedure employed for GB and GHCP, the GHCP, GB and LP have close $D_{5\%}$ and $D_{95\%}$ values (corresponding to the mesh dimensions through which respectively 5% and 95% of the powder are passing).

Specific surface areas (SSA) determined with the different methods for powders are presented in Table 2. There is a large difference of SSA with the BET and Blaine methods between GHCP and LP, GHCP having a much larger SSA than LP. On the contrary, the computed SSA for LP and GHCP are approximatively the same. In the case of computed SSA, the two powders are assumed to be composed of non-porous spherical particles. As the PSD of GHCP and LP are similar, the computed SSA are close for the two powders. On the contrary, BET and Blaine methods consider the real shape and surface roughness of particles, as well as part of their internal porosity. In that case, the SSA (Blaine or BET) of LP is much lower than that of GHCP because of the internal porosity of GHCP (capillary porosity and C–S–H porosity). This result confirms the fact that pores are still present in GHCP after grinding.

A small difference is observed for SSA (Computed, Blaine and BET) between LP and GB. This can probably be attributed to the opening of brick's porosity during grinding, the SSA being in that case essentially related to particles sizes.

3 Modeling approach

3.1 Presentation of the model

The original model presented in this section allows the estimation of the remaining porosity of a ground porous material. The latter is fed by the pore size distribution of the monolith porous material and the PSD of the ground powder. The following hypotheses are made:

1. The porous network is considered as homogeneous and isotropic
2. Grains are considered spherical
3. Pores are decomposed as a set of individual pores, each being characterized by a center, a characteristic dimension r and a characteristic volume V_{cp} (Fig. 3)

Table 1 Porosity measured using MIP on the monolith HCP, and the standard deviations computed from 5 replicates

Test	ρ_{app} MIP (g/cm^3)	Porosity MIP (%)	ρ MIP (g/cm^3)
HCP			
1	2.1	24.81	1.58
2	2.12	27.43	1.54
3	2.13	25.15	1.59
4	2.11	26.1	1.56
5	2.12	26.22	1.57
Average	2.12 ± 0.01	25.9 ± 0.8	1.57
Brick			
1	2.76	30.14	1.93
2	2.85	31.05	1.96
3	2.85	30.3	1.98
4	2.88	31.32	1.97
5	2.82	30.01	1.98
Average	2.82 ± 0.01	30 ± 0.6	1.98
LP[a]	2.72[a]	1[a]	2.72[a]

[a]Result obtained on the monolith LP according to the manufacturer

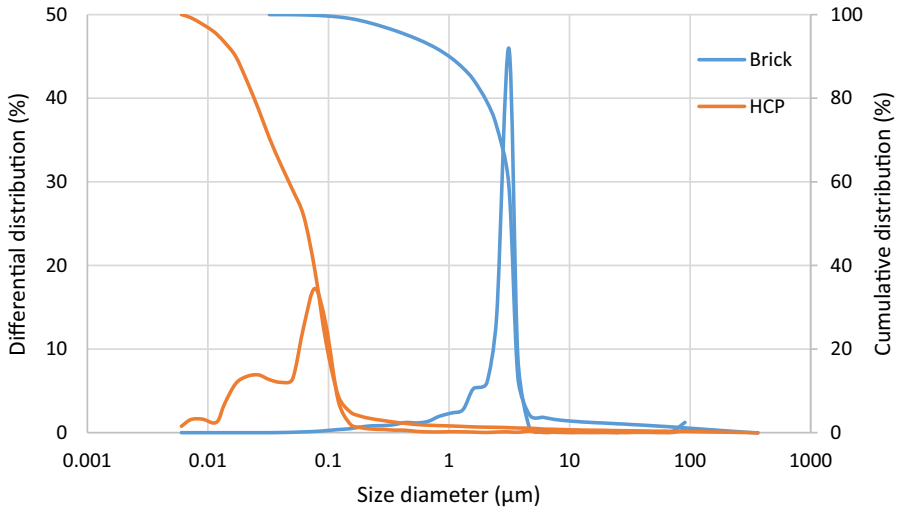

Fig. 1 Pore size distributions of the monolith HCP and brick

4. The pore is considered open if it is cut by the particle's surface and if it is larger than a diameter which correspond to the smallest intergranular pore (this hypothesis is discussed below).

In order to compute the remaining porosity of the powder, the distinction between inter-granular and intra-granular porosity should be made in the theoretical model. A pore located at the surface of a new-ground particle will be in direct contact with the inter-granular porosity. The question if this pore has to be considered as an inter-granular or an intra-granular void is arbitrary. In the following, we consider that a pore which diameter is larger or equal to the smallest inter-granular void of the packing belongs to the inter-granular porosity. On the contrary, pores that are smaller than the smallest inter-granular voids are counted with the intra-granular porosity. Figure 4 illustrate 3 neighboring particles in a packing of monosized spherical grains of radius R. The smallest pore of the packing corresponds to bottlenecks between three touching particles, which radius is equal to $0.1547 \times R$. So, all the pores present at the surface of ground particles which radius is larger than $0.1547 \times R$ will be considered, in the model, as new inter-granular pores.

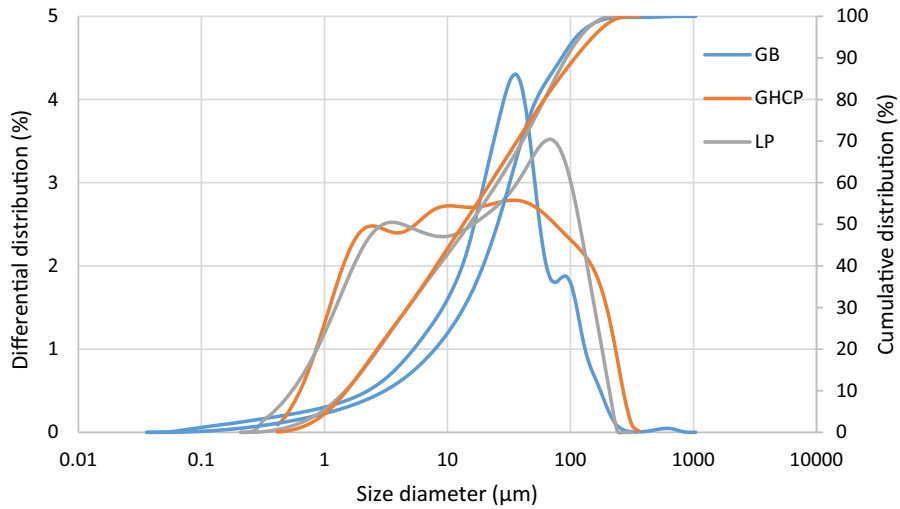

Fig. 2 Particle size distributions of GB, GHCP and LP

Table 2 Specific surface areas for GB, GHCP and LP

	GB	GHCP	LP
SSA Blaine (cm^2/g)	3282	9499	3180
SSA BET (cm^2/g)	10,000	90,000	8000
SSA Computed (cm^2/g)	4572	5244	4972

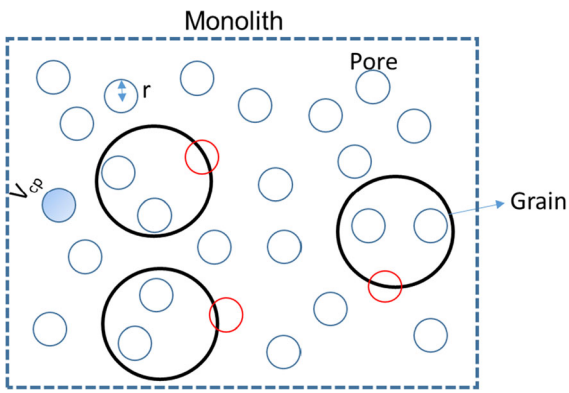

Fig. 3 Illustration of the pore network and the grinding procedure. r is the characteristic dimension of the pore, and $V_{cp,}$ is the volume of pore. Red pores correspond to those opened during the grinding procedure

First, we consider only one size of spherical grain of radius R and one characteristic size of pore r larger than the radius of the smallest inter-granular pore ($0.1547 \times R$). The density of pore centers (ρ_c) can be defined with (Eq. 2), where dN_c represents the number of pore centers in an elementary volume dV, and ϕ the initial porosity.

$$\rho_c = \frac{dN_c}{dV} = \frac{\phi}{V_{cp}} \tag{2}$$

The elementary volume of pores dV_p can be calculated in a volume of particle dV when $dV > > V_{cp}$ according to (Eq. 3).

$$dV_p = dN_c V_{cp} = r_c V_{cp} dV \tag{3}$$

$dV > > V_{cp}$ means that the volume on which the porosity is calculated is very large in front of the elementary volume of the pore. But that does not mean that it is a single volume, it can be the cumulative volume of a very large number of small grains.

The remaining pore volume (V_p) in a particle of radius R corresponds to the porosity of all pores whose centers are located at a distance from the center of the grain smaller than $R-r$ (Fig. 5), excluding all the pores that are cut from the surface of the grain. (Eqs. 4 and 5) present the volume of remaining pores in the particle after grinding.

$$V_p = \int_0^{R-r} dV_p = \int_0^{R-r} \rho_c V_{cp} dV \tag{4}$$

$$V_p = \int_0^{R-r} \frac{\phi}{V_{cp}} V_{cp} dV = \int_0^{R-r} \phi dV = \phi \frac{4\pi}{3} \left(R^3 - 3R^2 r + 3Rr^2 - r^3\right) \tag{5}$$

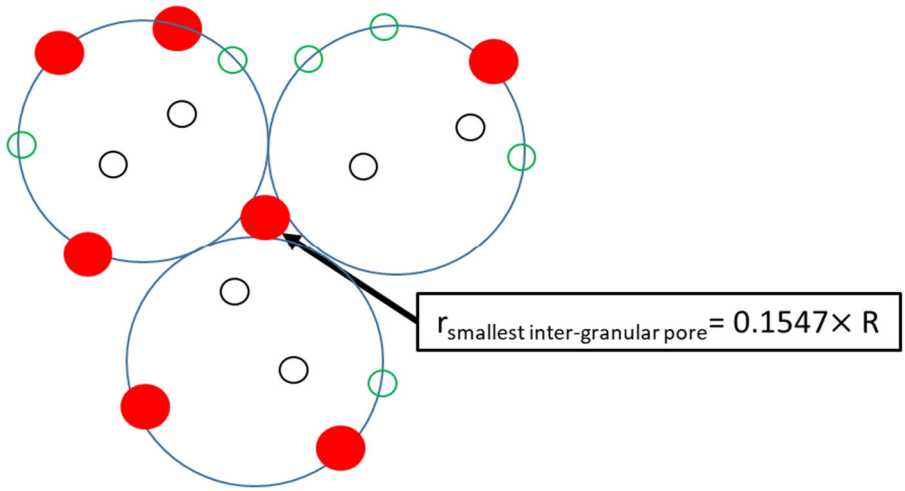

Fig. 4 Illustration of the smallest inter-granular pore in a packing of monosized spherical particles. Pores in red are larger than the smallest inter-granular pore, so they are not considered in the calculation of the intra-granular porosity

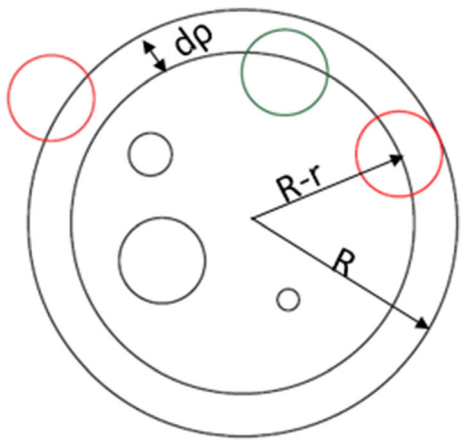

Fig. 5 Illustration of pores that are excluded due to the grinding procedure

The remaining porosity (ϕ_r) of the material after grinding is finally given by (Eq. 6).

$$\phi_r = \frac{V_p}{V_{\text{grain}}} = \phi \times \left(1 - 3\left(\frac{r}{R}\right) + 3\left(\frac{r}{R}\right)^2 - \left(\frac{r}{R}\right)^3\right) \tag{6}$$

Equation 6 allows to compute the remaining porosity when only one size of pores and one size of particles are taken into consideration (if $r \geq 0.1547$ R). Pores that are smaller than 0.1547 R might also be "split" in two parts during grinding, but in that case, they will still be considered as intra-granular pores so there will be no reduction for the intra-granular porosity of the powder with respect to the monolith material. In order to calculate the remaining porosity of one size of grain taking into consideration all the pore sizes (or radii r_i), (Eq. 6) has to be cumulated over all pore sizes (Eq. 7), considering the volume fraction of each size of pores (x_i). If a pore is larger than 0.1547 $\times$ R, the porosity is eliminated by grinding.

$$\phi_r = \phi \times \left\{\sum_{i=0}^{m} x_i + \sum_{i=m+1}^{n} x_i \times \left(1 - 3\left(\frac{r_i}{R}\right) + 3\left(\frac{r_i}{R}\right)^2 - \left(\frac{r_i}{R}\right)^3\right)\right\} \tag{7}$$

$$\text{with } \begin{array}{c} r_i < r_{i+1}, for i = 1 \text{to} i = n \\ r_m < 0.1547 \times R \text{ and } r_{m+1} \geq 0.1547 \times R \end{array}$$

Finally to compute the remaining porosity of the material for all sizes of grains (R_j), (Eq. 8) should be multiplied by the volume fraction of each size of grain (y_j). Where $R_{5\%}$ coresponds to the radius of 5% of the passing particle.

$$\phi_r = \phi \times \sum_{j=0}^{k} y_j \times \left\{\sum_{i=0}^{m} x_i + \sum_{i=m+1}^{n} x_i \times \left(1 - 3\left(\frac{r_i}{R_j}\right) + 3\left(\frac{r_i}{R_J}\right)^2 - \left(\frac{r_i}{R_j}\right)^3\right)\right\} \tag{8}$$

$$\text{With } \begin{array}{c} r_i < r_{i+1}, \quad \text{for } i = 1 \text{ to } i = n \\ r_m < 0.1547 \times R_{5\%} \text{ and } r_{m+1} \geq 0.1547 \times R_{5\%} \end{array}$$

3.2 Application of the theoretical model to GHCP and GB

First the theoretical model has been applied to the GB and GHCP. The PSDs of the powders and the pore size distributions of the monoliths are considered as input data for the model. The performed MIP test in various samples of HCP and brick (monolith) showed that HCP and brick are homogeneous. The eventual cracks initially present in the monoliths (HCP and brick) are considered as pore, and they are considered in the initial porosity. However, it is not possible to estimate the additional porosity caused during the grinding procedure, so we have to neglect the latter in the model.

In order to obtain the final porosity after grinding HCP and Brick, (Eq. 8) is used. The smallest inter granular pore of each material has to be defined. In the following, the value coresponding to $0.1547 \times R_{5\%}$ has been retained, where $R_{5\%}$ coresponds to the radius of 5% of the passing particle. This radius is considered as the smallest grain radius of both GHCP and GB.

The remaining porosity of GHCP is 24.7%. A difference of 1.2% in the porosity between HCP and GHCP is observed. The remaining porosity of GB is 2%. A difference of 28% in the porosity between the monolith brick and GB is obtained. This difference in the porosity of the monolith and the powder is due to the opening of pores during the grinding procedure. The difference in the remaining porosity between GHCP and GB is attributed to the difference of the size of pores of the monolith HCP and brick (Fig. 1).

4 Experimental approach

4.1 MIP analyses of LP

Several authors already used MIP to study the compaction of powders [34, 35]. According to Guerin et al. [36] there are two distinct zones in the resulting MIP curve on powders. The first one corresponds to the compaction of the granular stack under the action of the pressure increase, going from the random loose to a random closer packing [37]. The second one refers to the progressive filling of inter granular pore volume by mercury.

Figure 6 presents the variation of the packing density (γ_{total}) as a function of the diameter of pores for LP when using MIP. The packing density (γ_{total}) is expressed according to (Eq. 9), where V_s is the solid volume of LP, and $V_0 - V_{\text{inject}}$ is the total volume of the packing for a given pressure of mercury.

$$\gamma_{\text{total}} = \frac{V_S}{V_0 - V_{\text{inject}}} \tag{9}$$

To identify the first zone where only compaction occurs because of the filling of large compaction voids, a model of compaction dynamics is used. The compaction dynamics of granular materials has been extensively studied in the literature [37–39]. It has been shown that the packing density of a granular material subjected to compaction evolves as a function of time according to (Eq. 10):

$$\gamma(t) = \gamma_\infty - \Delta\gamma_\infty \times \exp\left(-\left(\frac{t}{\tau}\right)^\beta\right) \tag{10}$$

where γ_∞ is the final packing density, $\Delta\gamma_\infty$ corresponds to the variation of packing density during compaction, t is the number of taps applied to the powder, τ is a characteristic time, and β a fitting parameter. It has been shown that this relation can be generally used to describe the compaction dynamics of granular materials [39]. In this research, we apply (Eq. 10) to characterize the first zone of the MIP on powders, replacing the number of taps t by the pressure of mercury (expressed as pore diameters in Fig. 6). The application of the compaction dynamics model needs the use of the envelope volume of grains (V_{envelope}), taking into account intra granular porosity. LP being quasi non-porous, the solid volume V_s is considered equal to V_{envelope}.

Equation 10 is used here in order to describe the first zone of the curve. It has therefore been fitted to the MIP results from the beginning of the test up to a certain pressure (or pore radius) corresponding to the end of compaction. As long as (Eq. 10) allows for a good fitting of MIP results with fitting parameters that are meaningful, we can consider that the compaction zone is not completed. Table 3 presents the fitting parameters obtained for different applied pressures when using the compaction model. It can be seen that, for a pore radius of 2.46 µm, γ_∞ is larger than unity, which has no physical meaning. On the contrary, the fitting parameters obtained for a pore radius of 3.08 µm are coherent and the fitting of the model is good ($R^2 = 0.98$) and shows that (Eq. 10) can be used

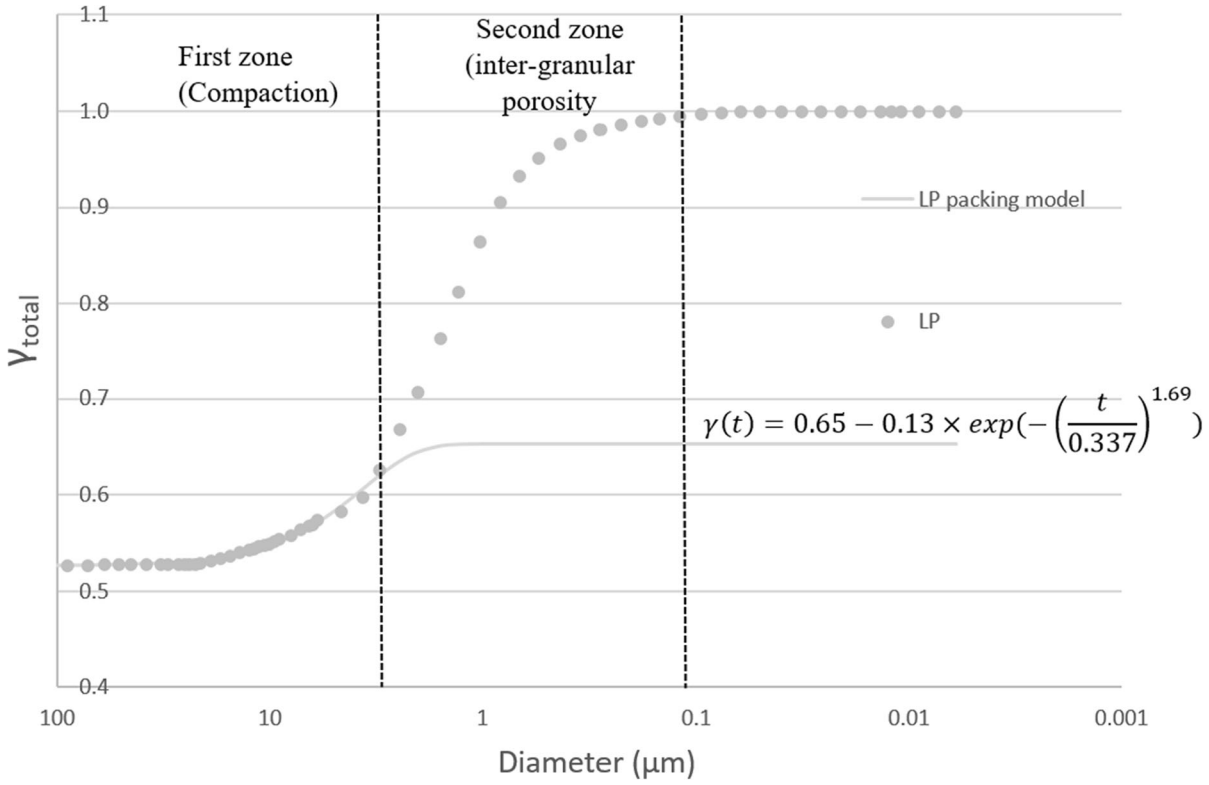

Fig. 6 Variation of γ_{total} as a function of pore diameter for LP. There is a direct relation between the pore size and the pressure, when the pressure increases the pore diameter decreases. That's why, the pore size is presented in reversed way

Table 3 Fitting parameters obtained when using Eq. 10 to identify the compaction zone for LP

Pressure (MPa)	Pore diameter (µm)	γ_∞	τ (MPa)	B	R^2
0.268	4.63	0.59	0.165	2.34	0.994
0.337	3.69	0.60	0.199	2.09	0.993
0.399	3.08	0.65	0.337	1.69	0.986
0.503	2.46	1.53	2.02	1.39	0.993

to describe the compaction of powders under an increasing pressure of mercury. It is therefore considered that the end of the first zone corresponds to 3 µm. In this zone, the packing density of LP powder increases from a packing density of 0.52 (random loose packing) to 0.65 (random close packing).

According to Guerin et al. [36], the second zone corresponds to the progressive filling of inter-granular pore volume. As mentioned in the theoretical model, we consider that the smallest inter-granular pore is $0.1548 \times D_{5\%}$, where $D_{5\%}$ is equal to 1.04 µm for LP. Therefore the smallest inter-granular pore is equal to 0.16 µm. The intra granular porosity of LP is 1%, which is close to the one of the monolith LP (according to the manufacturer).

4.2 MIP analysis on GHCP and GB

Figure 7 illustrates the different volumes considered when using MIP to analyze a porous powder. V_S is the solid volume of particles. V_0 is the initial apparent volume of the powder, $V_{injected}$ is the volume of injected mercury, V_{comp} corresponds to the compacted volume obtained during the transition from random loose to random closer packing (first zone) and V_{inter} is the inter-granular volume. In the case of a porous powder, an additional volume corresponding to the

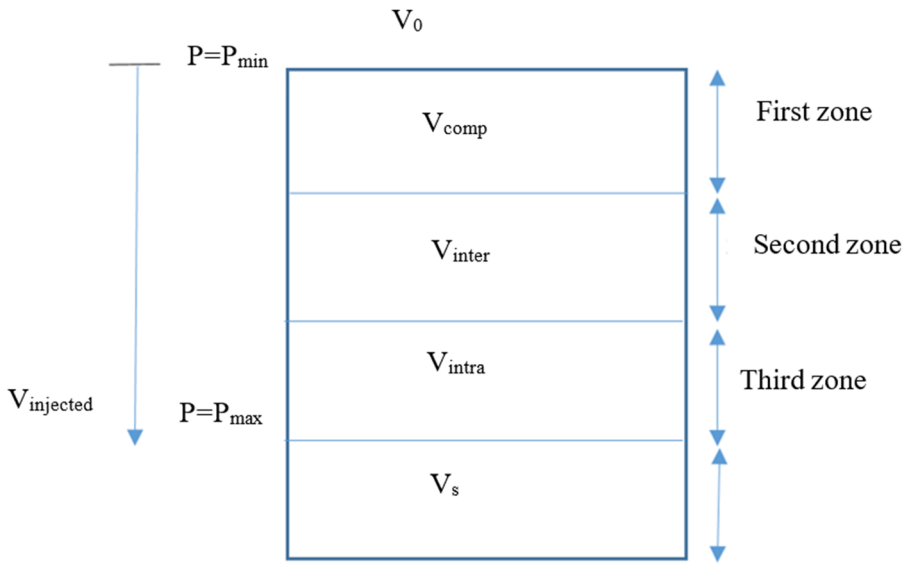

Fig. 7 Illustration of the different volumes when using MIP analyses on a porous powder. The different volumes correspond to decreasing sizes of pores. *P* corresponds to the mercury pressure

intra-granular porosity that is accessible to mercury has to be added V_{intra}.

Figure 8 presents the variation of γ_{total} as a function of the diameter of pores for LP, GB and GHCP. The diameter of the smallest intergranular pore of GB is equal to 0.18 µm and for GHCP is equal to 0.17 µm.

Equation 10 (Eq. 10) has been used to identify the first zone corresponding to the compaction of both GB and GHCP particles. The envelope volume has to be computed according to (Eq. 11). Then, dynamics of compaction (Eq. 10) has to be fitted not to the total packing density but to envelop packing density (Eq. 13).

$$V_{\text{envelope}} = V_{\text{s}} + V_{\text{intra}} \tag{11}$$

$$\gamma_{R_{5\%}} = \frac{V_S}{V_S + V_{\text{intra}}} \tag{12}$$

$$\gamma_{\text{envelop}} = \frac{V_{\text{envelop}}}{V_0 - V_{\text{inject}}} = \frac{V_{\text{S}} + V_{\text{intra}}}{V_0 - V_{\text{inject}}} = \gamma_{\text{total}} + \frac{V_{\text{intra}}}{V_0 - V_{\text{inject}}}$$
$$= \gamma_{\text{total}} + \frac{V_{\text{S}}}{V_0 - V_{\text{inject}}} \times \left(\frac{1}{\gamma_{R_{5\%}}} - 1 \right)$$
$$\gamma_{\text{envelop}} = \frac{\gamma_{\text{total}}}{\gamma_{R_{5\%}}} \tag{13}$$

Table 4 presents the fitting parameters for different applied pressures for GHCP when using the compaction model. For a pore diameter of 1.59 µm, the description of the first part of the curve is not satisfying (R^2 = 0.94), and it is therefore considered that the end of the compaction zone is reached for a pore diameter of 2 µm (R^2 = 0.989). This upper limit diameter is close to the one obtained for LP (3 µm).

Table 5 presents the fitting parameters for different applied pressure for GB when using the compaction model. For a pore radius of 4.66 µm, γ_∞ is larger than unity, which has no physical sense. On the contrary, the fitting parameters obtained for a pore radius of 6.03 µm are coherent and the fitting of the model is good (R^2 = 0.99).

The packing density obtained with (Eq. 13) of GHCP increases from 0.607 (random loose packing) to 0.76 (random close packing), and for GB increases from 0.433 (random loose packing) to 0.51 (random close packing).

The evolution of γ_{total} in the second zone (inter granular porosity) differs significantly between LP and GHCP. The difference can be attributed to the unequivalent packing density of both materials, when GHCP has a larger packing density than LP. There is a small difference in the evolution of γ_{total} in the second zone (inter granular porosity) between LP and GB, this

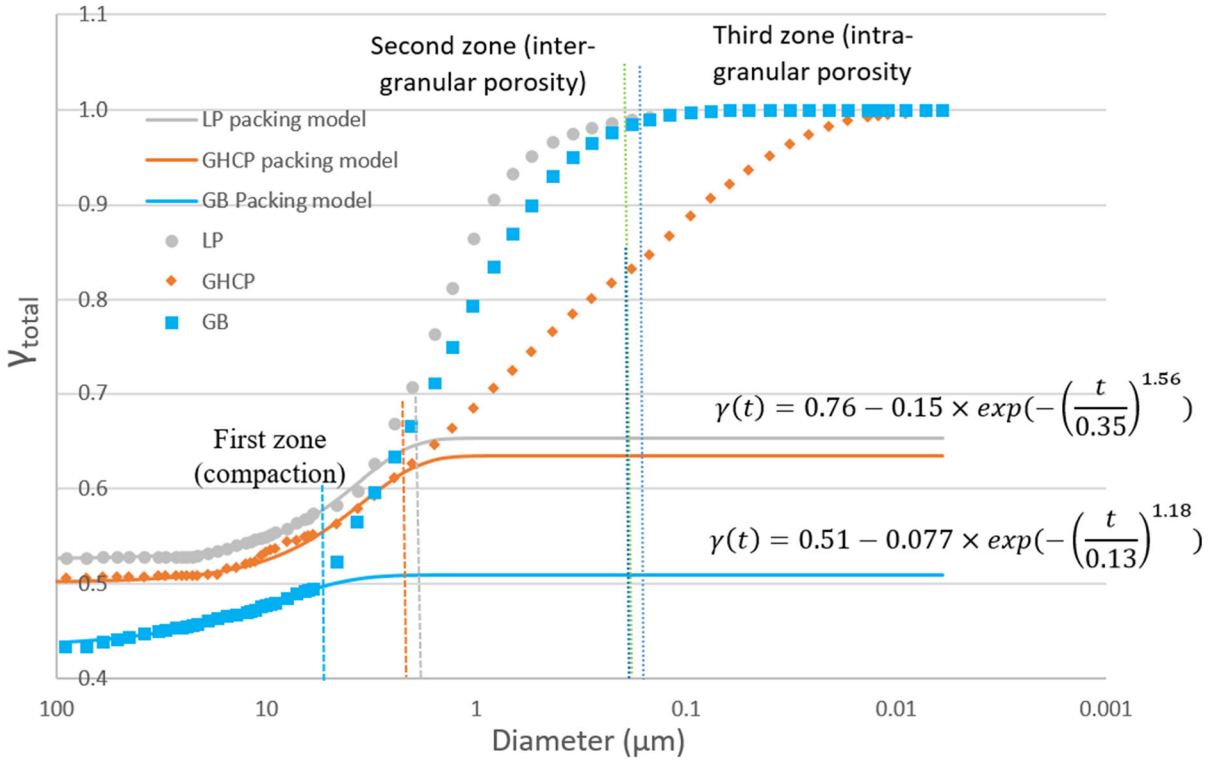

Fig. 8 Variation of γ_{total} as a function of the pore diameter for LP, GHCP and GB. There is a direct relation between the pore size and the pressure, when the pressure increases the pore diameter decreases. That's why, the pore size is presented in reversed way

Table 4 Fitting parameters obtained when using Eq. 10 to identify the compaction zone for GHCP

Pressure (MPa)	Pore diameter (µm)	γ_∞	τ (MPa)	B	R^2
0.399	3.08	0.71	0.24	1.89	0.983
0.503	2.46	0.74	0.29	1.67	0.985
0.606	2.04	0.76	0.35	1.56	0.988
0.779	1.59	0.79	0.43	1.44	0.949

Table 5 Fitting parameters obtained when using Eq. 10 to identify the compaction zone for GB

Pressure (MPa)	Pore diameter (µm)	γ_∞	τ (MPa)	β	R^2
0.18	6.58	0.50	0.12	1.21	0.99
0.19	6.29	0.51	0.13	1.19	0.99
0.2	6.03	0.51	0.13	1.18	0.99
0.26	4.66	1.13	2.73	0.89	0.98

difference can be caused by the fact that the filling of the inter-granular porosity start at 4 µm for GB, where the one of the LP start at 2 µm.

Finally, the third zone allows us to compute the intra granular porosity of GB and GHCP This value can be computed with (Eq. 14) and is equal to 16.5% for GHCP, and 2.1% for GB.

$$\text{Intra-granular porosity} = 1 - \gamma_{R_{5\%}} \quad (14)$$

5 Comparison between the experimental and theoretical approaches

Table 6 presents the initial porosity of the monolith material and the remaining porosities obtained with the theoretical model and experimentation.

The difference between initial and remaining porosities largely depends on the type of material. For GHCP, the remaining porosity after grinding is still very high (24.7% with the model and 16.7% with MIP). On the contrary, for GB, the porosity is almost eliminated by the grinding procedure (2% and 2.1% respectively with the model and MIP). This result can be explained by the ratio between the size of pores to the size of grains of the two materials. As expected, when the size of pores is very small in comparison to the size of grains, grinding do not eliminate a lot of porosity (case of the GHCP). On the contrary, when the size of pores is close to that of grains (as for GB), grinding leads to an opening of the majority of pores which transforms intragranular pores into intergranular.

Moreover, for the GHCP, the porosity obtained by the experimental approach is significantly smaller than that obtained with the model. For this material, when the pressure of mercury is large enough so that it can enter pores of radius ($0.1547 \times R_{5\%} = 0.18$ µm), mercury will penetrate deeper in the particles as long as the pore radius is larger than or equal to 0.18 µm.(which is considered in that case as intergranular porosity). Even if the volume of pores larger than or equal to 0.18µm is small (about 4% measured on the monolith in Fig. 1), it could be significantly larger in the ground material. Indeed, MIP tends to underestimate the fractions of large pores because of the "bottle of ink" shaped pores, with an inlet diameter narrower than the diameter of the pore itself. When the material is ground, the large increase in surface area of the powder comparatively too the monolith certainly opens an access to a larger amount of large pores and decreases the influence of "bottle of inks" on the result. According to that, the model, which is based on the MIP on the monolith overestimates the remaining porosity, whereas the experimental procedure underestimates it for GHCP.

On the contrary, the porosity of GB obtained with the experimental approach is 2.1% which is very close to the value predicted by the theoretical one (2%). In that case, the size of pores is much closer to the size of particles, therefore, grinding eliminates a lot of pores. Figure 1 shows that 2% of the porosity is smaller than 0.1547 x $R_{5\%}$, this value is close to those obtained by the two procedures. In that case, the major part of the pores is eliminated by grinding, even more for "bottle of inks" pores which are larger than entry pores on the monolith.

Whatever the method used, the porosity of the GHCP is still high. Thus, it is clear that grinding a monolith porous material does not eliminate all the porosity if the size of particles is much larger than the size of pores.

To conclude, the parameter which controls the remaining porosity is the ratio between the size of pores and the size of grains. In the case of brick, the size of pores in the monolith is close to the size of grains of GB, so a large part of porosity is eliminated, and both theoretical and experimental methods give similar results. In these conditions, both methods can be employed, depending on the data available. For GHCP, the two methods give different results, which can be attributed both to the much smaller size of pores than size of particles and to the pores in bottle of ink shape which are more present in the monolith than in the ground material. In that case, the result given by the experimental approach are underestimated, whereas those of the model are certainly overestimated. However, it is preferable to use the model instead of the experimental approach for these kind of materials as MIP seems to largely underestimate the remaining porosity. But it is needed to have the pore size distribution before grinding for applying the theoretical model, which is not always possible. In that

Table 6 Comparison between the remaining porosity obtained with theoretical model and experimental procedure

	Initial porosity (%)	Theoretical model (%)	Experimentation (%)
GHCP	25.9	24.7	16.7
GB	30	2	2.1

case, the experimental method can be used, and it should be kept in mind that the final result is underestimated. As mentioned in part 1, there is actually no alternative method allowing the measurement of this porosity.

6 Conclusion

Two approaches, theoretical and experimental have been presented in this paper to estimate the remaining intra granular porosity of a material addition after grinding.

An original model has been developed in order to compute the remaining porosity of porous powders. This model is fed by the pore size distribution obtained for the monolith porous material and the particle size distribution obtained after being ground.

An experimental procedure based on MIP on powders has also been developed to estimate their inter and intra-granular porosities. Inter granular porosity is first identified with a model of compaction dynamics that can be fitted on the mercury intrusion curve at low pressure. The end of the inter-granular porosity zone is identified with the smallest inter granular pore, then after the intra-granular porosity of the particles can be deduced.

The two approaches have been applied on ground hardened cement paste and brick. The results suggest that:

- The major part of the porosity of the brick is eliminated by grinding, which is not the case for the GHCP. This is explained by the fact that the size of pores and size of grains are close in GB, which is not the case of GHCP, where the smallest grain ($R_{5\%}$) is 10 times bigger than the largest pore.
- The of bottle of ink-shaped pores are more abundant in the monolith than in the powder due to the increase in surface area connected with mercury in the latter, which can explain the differences on porosity between the two approaches on the GHCP.
- The theoretical model certainly overestimates a bit the remaining porosity and the experimental method underestimates it. When possible, the modeling approach has to be preferred because of the difficult interpretation of experimental results of MIP on powders and of the underestimation of remaining porosity.

The next step of this research is to study the effect of using a porous powder as mineral addition, and the effect of its porosity in the fresh and hardened behavior properties on mortars or concrete.

Acknowledgements This research work has been carried out in the frame of the VALDEM project (convention no. 1.1.57 of Interreg France-Wallonie-Vlaanderen 2014-2020), partly financed by the European Regional Development Funds and Wallonia.

Compliance with ethical standards

Conflict of interest The authors declare that they have no conflicts of interest.

References

1. Kajaste R, Hurme M (2016) Cement industry greenhouse gas emissions—management options and abatement cost. J Clean Prod 112:4041–4052. https://doi.org/10.1016/j.jclepro.2015.07.055
2. Habert G, Roussel N (2009) Study of two concrete mix-design strategies to reach carbon mitigation objectives. Cem Concr Compos 31(6):397–402. https://doi.org/10.1016/j.cemconcomp.2009.04.001
3. Habert G, Roussel N (2008) Comment concevoir un béton ayant un faible impact environnemental? XXVIemes Rencontres Univ. Génie Civ. AUGC 2008
4. Diliberto C, Lecomte A, Mechling J-M, Izoret L, Smith A (2017) Valorisation of recycled concrete sands in cement raw meal for cement production. Mater Struct 50(2):127. https://doi.org/10.1617/s11527-017-0996-8
5. Khoury E, Ambrós W, Cazacliu B, Sampaio CH, Remond S (2018) Heterogeneity of recycled concrete aggregates, an intrinsic variability. Constr Build Mater 175:705–713. https://doi.org/10.1016/j.conbuildmat.2018.04.163
6. Colman C, Bulteel D, Rémond S, Zhao Z, Courard L (2020) Valorization of fine recycled aggregates contaminated with gypsum residues: characterization and evaluation of the risk for secondary ettringite formation. Materials (Basel) 13(21):1–12. https://doi.org/10.3390/ma13214866
7. Colman C, Bulteel D, Thiery V, Rémond S, Michel F, Courard L (2021) Internal sulfate attack in mortars containing contaminated fine recycled concrete aggregates. Constr Build Mater 272:121851. https://doi.org/10.1016/j.conbuildmat.2020.121851
8. Evangelista L, de Brito J (2007) Mechanical behaviour of concrete made with fine recycled concrete aggregates. Cem Concr Compos 29(5):397–401. https://doi.org/10.1016/j.cemconcomp.2006.12.004
9. Evangelista L, de Brito J (2010) Durability performance of concrete made with fine recycled concrete aggregates. Cem

Concr Compos 32(1):9–14. https://doi.org/10.1016/j.cemconcomp.2009.09.005
10. Carro-López D, González-Fonteboa B, De Brito J, Martínez-Abella F, González-Taboada I, Silva P (2015) Study of the rheology of self-compacting concrete with fine recycled concrete aggregates. Constr Build Mater 96:491–501. https://doi.org/10.1016/j.conbuildmat.2015.08.091
11. Evangelista L, Guedes M, De Brito J, Ferro AC, Pereira MF (2015) Physical, chemical and mineralogical properties of fine recycled aggregates made from concrete waste. Constr Build Mater 86:178–188. https://doi.org/10.1016/j.conbuildmat.2015.03.112
12. Bouarroudj ME, Remond S, Michel F, Zhao Z, Bulteel D, Courard L (2019) Use of a reference limestone fine aggregate to study the fresh and hard behavior of mortar made with recycled fine aggregate. Mater Struct. https://doi.org/10.1617/s11527-019-1325-1
13. Omary S, Ghorbel E, Wardeh G, Minh B, Nguyen D (2017) Mix design and recycled aggregates effects on the concrete's properties. Int J Civ Eng 8(16):973–992. https://doi.org/10.1007/s40999-017-0247-y
14. Oksri-Nelfia L, Mahieux P, Amiri O, Turcry P, Lux J (2016) Reuse of recycled crushed concrete fines as mineral addition in cementitious materials. Mater Struct 49(8):3239–3251. https://doi.org/10.1617/s11527-015-0716-1
15. Bordy A, Younsi A, Aggoun S, Fiorio B (2017) Cement substitution by a recycled cement paste fine: role of the residual anhydrous clinker. Constr Build Mater 132:1–8. https://doi.org/10.1016/j.conbuildmat.2016.11.080
16. Krour H, Trauchessec R, Lecomte A, Diliberto C, Barnes-Davin L, Bolze B, Delhay A (2020) Incorporation rate of recycled aggregates in cement raw meals. Constr Build Mater 248:118217. https://doi.org/10.1016/j.conbuildmat.2020.118217
17. Kapoor K, Singh SP, Singh B (2016) Durability of self-compacting concrete made with recycled concrete aggregates and mineral admixtures. Constr Build Mater 128:67–76. https://doi.org/10.1016/j.conbuildmat.2016.10.026
18. PN R (2012) Complete recycling of concrete. http://www.pnrecybeton.fr/.
19. Neville A (1988) Properties of concrete
20. Williams DA, Saaka AW, Jennings HM (1999) The influence of mixing on the rheology of fresh cement. Cem Concr Res 29:1491–1496
21. Bouarroudj M, Bulteel D, Potier G, Michel F, Zhao Z, Courard L (2020) Use of grinded hardened cement pastes as mineral addition for mortars. J Build Eng. https://doi.org/10.1016/j.jobe.2020.101863
22. E. 1097-6 (2013) Tests for mechanical and physical properties of aggregates—part 6: determination of particle density and water absorption
23. ASTM C 128–04 (2004) Standard test method for density, relative density (specific gravity), and absorption of fine aggregate
24. IFSTTAR. Test Methode No.78 (2011) Tests on granulats in concrte: measurment of total water absorption of crushed sand
25. Zhao Z, Remond S, Damidot D, Xu W (2013) Influence of hardened cement paste content on the water absorption of fine recycled concrete aggregates. J Sustain Cem Mater 2(3–4):186–203. https://doi.org/10.1080/21650373.2013.812942
26. Le T, Rémond S, Le Saout G, Garcia-Diaz E (2016) Fresh behavior of mortar based on recycled sand—influence of moisture condition. Constr Build Mater 106:35–42. https://doi.org/10.1016/j.conbuildmat.2015.12.071
27. Hedenus P, Strømme Mattsson M, Niklasson GA, Camber O, Ek R (2000) Characterisation of instantaneous water absorption properties of pharmaceutical excipients. Int J Pharm 202(1–2):141–149. https://doi.org/10.1016/S0378-5173(00)00436-1
28. Strømme Mattsson M, Hedenus P, Niklasson GA, Ek R (2000) A new method of characterising liquid uptake within particles over short time periods. Int J Pharm 199(2):179–185. https://doi.org/10.1016/S0378-5173(00)00381-1
29. EN 197-1 (2012) Cement—part 1: composition, specifications and conformity criteria for common cements
30. Frías M, Cabrera J (2000) Pore size distribution and degree of hydration of metakaolin-cement pastes. Cem Concr Res 30(4):561–569. https://doi.org/10.1016/S0008-8846(00)00203-9
31. Bentz DP (2006) Quantitative comparison of real and CEMHYD3D model microstructures using correlation functions. Cem Concr Res 36(2):259–263. https://doi.org/10.1016/j.cemconres.2005.07.003
32. M. Cyr (1999) Contribution à la caractérisation des fines minérales et à la compréhension de leur rôle joué dans le comportement rhéologique des matrices cimentaires. université de sherbrooke
33. E. 196-6 (2018) Methods of testing cement—determination of fineness
34. Westermarck S (2000) Use of mercury porosimetry and nitrogen adsorption in characterisation of the pore structure of mannitol and microcrystalline cellulose powders, granules and tablets
35. Westermarck S, Juppo AM, Kervinen L, Yliruusi J (1998) Pore structure and surface area of mannitol powder, granules and tablets determined with mercury porosimetry and nitrogen adsorption. Eur J Pharm Biopharm 46(1):61–68. https://doi.org/10.1016/S0939-6411(97)00169-0
36. Guerin E, Tchoreloff P, Leclerc B, Tanguy D, Deleuil M, Couarraze G (1999) Rheological characterization of pharmaceutical powders using tap testing, shear cell and mercury porosimeter. Int J Pharm 189(1):91–103. https://doi.org/10.1016/S0378-5173(99)00243-4
37. Rémond S (2004) Compaction of confined mono-sized spherical particle systems under symmetric vibration: a suspension model. Phys A Stat Mech Appl 337(3–4):411–427. https://doi.org/10.1016/j.physa.2004.02.014
38. Richard P, Nicodemi M, Delannay R, Ribière P, Bideau D (2005) Slow relaxation and compaction of granular systems. Nat Mater 4:121–128
39. Rémond S, Gallias JL (2006) Simulation of periodic mono-sized hard sphere systems under different vibration conditions and resulting compaction. Phys A Stat Mech Appl 369(2):545–561. https://doi.org/10.1016/j.physa.2006.01.071